Aerospace Science and Technology 98 (2020) 105716

Contents lists available at ScienceDirect

Aerospace Science and Technology

www.elsevier.com/locate/aescte

Nonsingular terminal sliding mode control for a quadrotor UAV with a total rotor failure

Zhiwei Hou, Peng Lu *, Zhangjie Tu

Interdisciplinary Division of Aeronautical and Aviation Engineering, the Hong Kong Polytechnic University, Hong Kong, China

ARTICLE INFO

Article history:
Received 17 June 2019
Received in revised form 2 December 2019
Accepted 16 January 2020
Available online 22 January 2020
Communicated by Christian Circi

Keywords:
Quadrotor UAV
Terminal sliding mode control
Fault-tolerant control
Model uncertainty
Wind disturbance

ABSTRACT

Based on nonsingular terminal sliding mode control (NTSMC), a flight controller is proposed in this paper for a quadrotor with a total rotor failure. The proposed method is a finite-time position and attitude tracking approach with strong robustness. At first, the fault-tolerant controller for the quadrotor with a total rotor failure is derived, and the model uncertainties and wind disturbances are considered. The dynamic model of the quadrotor is introduced and divided into two control loops: the inner control loop and the outer control loop. Based on the division of the control system, the NTSMC based inner controller is designed which makes the attitude dynamics converge to the desired attitude in finite-time. And the NTSMC based outer controller is derived which generates the desired attitude for the inner controller and makes the dynamics converge to the desired position in finite-time. The stability of the closed-loop system is analyzed by Lyapunov theory and the stability conditions are obtained. Then, in order to improve the practicability of the control algorithm, a flight controller for a fault-free quadrotor is proposed which has a similar structure compared with the fault-tolerant one. A fault detection and isolation method is applied to detect the fault and reconfigure the flight controllers. Moreover, two estimation methods for external disturbance and model uncertainties are applied to enhance the robustness of the proposed flight controller. The estimated wind disturbances results are introduced into the outer controller to compensate for the effect of disturbance while the model uncertainties estimator is applied in the inner control loop. Finally, numerical simulation results show the great performance of the proposed flight control method.

1. Introduction

Unmanned Aerial Vehicles (UAVs) are increasingly being used in various fields including search and rescue. Nowadays they are more popularly used for commercial services such as aerial photography according to their stability. Quadrotor is one kind of the rotating wings UAVs. Compared with fixed wing UAVs and other kinds of large scale UAVs, quadrotors can break through the limitation of the runway and realize hover action and vertical takeoffs and landings. It has been widely applied in the military and economic field, such as aerial surveys, tactics reconnaissance, materials transportation and fire surveillance. It has the advantage of flexibility, portability and cheapness. However, the quadrotor also has the characteristics of nonlinearity, strong coupling and under-actuation. The flight control law of quadrotor UAVs has been a hot area of research for several years.

Classical control methods have been applied to deal with the quadrotor control problem, such as PID [1], [2], [3] and fuzzy PID [4]. Many modern control methods are also applied in the design of the quadrotor's flight control system. In [5], an integral predictive and nonlinear robust control strategy based on model predictive control and H_∞ control is presented. In [6], a L_1 adaptive controller with an optimized filter is applied for the quadrotor's position tracking problem. The proposed method has a strong robustness to modeling error and time delay. Reinforcement learning method has also been applied to design the quadrotor's flight controller, as studied in [7], [8] and [9]. A kernel-based regression learning strategy is applied in [9] to predict the error of the modeling and an adaptive control method is proposed based on reinforcement learning approach. In [10] and [11], sliding mode control strategy is developed to control the attitude and position of the quadrotor.

* Corresponding author.
E-mail address: peng.lu@polyu.edu.hk (P. Lu).

https://doi.org/10.1016/j.ast.2020.105716
1270-9638/

However, despite of the increasingly mature technologies developed for the quadrotor, they still have an increased risk of sensor or actuator failures. The failures might affect the reliability and safety of the quadrotor. Therefore, Fault Detection and Diagnosis (FDD) and Fault Tolerant Control (FTC) are becoming more and more important research areas about the quadrotor UAVs [12][13].

Partial or total rotor failures are the FTC scenarios studied in recent years. Rotor failures have been studied by a few researchers [12] [14] [15] [16]. The effect of rotor failures can be modeled as the loss of control effectiveness, and robust and adaptive control approaches are well developed for this type of failure. In [17], model reference adaptive control (MRAC) and PID are utilized to design the fault-tolerant controller. In [18], three different MRAC methods, called MIT rule MRAC, the Conventional MRAC and the Modified MRAC, are applied to deal with the fault-tolerant control problem.

However, most of the above papers only consider the partial rotor failure of the quadrotor UAVs. The case of total rotor failure is more dangerous for the quadrotor and more difficult to deal with. The quadrotor becomes an under-actuated system when one of the rotors has totally failed, and it is impossible to fully control the attitude of the quadrotor in such a situation. Some researchers [19,20] argued that trajectory tracking can not be achieved without full attitude control. Freddi, Lanzon and Longhi [21,22] first studied the problem of fault-tolerant control for quadrotors in the presence of one total rotor failure. They designed the flight controller by sacrificing the controllability of the yaw angle and the proposed flight control strategy can still make the quadrotor realize trajectory tracking. The feedback linearization control has been used to design the fault-tolerant controller in [21] and [22] and the quadrotor spins around a certain axis as a result of sacrificing the yaw angle. In [23], the author presents a periodic solution to solve the fault-tolerant control problem with rotor's total failure. A PID based approach is presented in [24] to deal with a total rotor failure control problem. With the same modeling assumption, in [25] a backstepping approach is proposed to cope with the total failure of a motor. A multi-loop hybrid nonlinear controller is designed in [26] in order to realize high-speed flight of a quadrotor with a total rotor failure. One common drawback of the above research results is that they do not take the FDD part into consideration or set the FDD part as ideal. In [27] a complete active fault-tolerant control system is proposed, which copes with not only fault detection and isolation but also fault-tolerant control.

Sliding mode control (SMC) has been widely studied and applied in different fields [28]. The traditional linear sliding mode control (LSMC) is well known for its strong robustness. However, LSMC is a asymptotically stable method, which means the states of the control system can't converge to the equilibrium point within a finite time after the sliding mode surface is reached. In [29], the concept of 'terminal attractor' is first proposed, and terminal sliding mode control (TSMC) is proposed as a result. With TSMC, the states of the system will converge to the equilibrium point in finite time. However, TSMC has the problem of singularity which means that the magnitude of the control input might be infinite large to guarantee the stability of the control system. An indirect way is proposed in [30] to deal with the singularity problem. In [31], nonsingular terminal sliding mode control (NTSMC) is first proposed by redesigning the sliding mode surface. In [32], NTSMC is further extended to the high-order systems. SMC has been widely applied in control engineering, such as missile's guidance law design [33], [34], [35] and [36], and vehicle's control strategy design [37]. In [38], a SMC based back-stepping method is proposed to deal with the external disturbance of the quadrotor. And in [39], the partial fault tolerant control problem of quadrotor is solved based on SMC and sliding mode disturbance observers.

Based on NTSMC, this paper proposes a fault-tolerant flight controller for the quadrotor UAV. The main contributions of this paper are stated as follows: 1) NTSMC is firstly applied to deal with the one rotor total failure problem of quadrotors, which means that one of the four rotors is totally broken and only three rotors can be utilized to control the quadrotor. Most of the existing fault-tolerant quadrotor flight controllers are designed to deal with the partial rotor failure problem, as in [12] and [14–18]. The proposed NTSMC based fault-tolerant flight controller is a finite-time convergent method with strong robustness. 2) The model uncertainties and external disturbances (wind) are considered in this paper with a total rotor failure. Two methods, sliding mode differentiator (SMD) [28] and nonlinear disturbance estimator (NDE) [40], are utilized to estimate the external disturbances and model uncertainties in real time. It is the first time that we use NDE to estimate the wind disturbance and model uncertainties acting on the quadrotor. The proposed NDE and SMD based NTSMC method shows strong robustness and better control performance compared with pure NTSMC method. We compare the NDE-based estimator with SMD and show that the NDE-based estimator is more insensitive to noise. 3) A complete fault-tolerant control system is studied in this paper, which copes with not only fault detection and diagnosis but also fault-tolerant control. Most existing works did not take the FDD part into consideration or set the FDD part as ideal, as in [21–26]. A flight controller for a fault-free quadrotor is proposed which has a similar structure compared with the fault-tolerant one. And a fault detection and isolation method is applied to detect the failure and reconfigure the flight controllers.

The rest of the paper is organized as follows. Section 2 describes the dynamic model of the quadrotor, including the fault-free model and fault-tolerant model. Section 3 designs the NTSMC based complete fault-tolerant control system, including the fault-tolerant controller, the fault-free controller, the FDD method and the external disturbances estimator. Section 4 shows the great performance of the proposed flight control method through numerical simulations. Conclusions are presented in Section 5.

2. Quadrotor model

The dynamical model of the quadrotor UAVs is shown in Fig. 1. Four independent motors on which propellers are fixed are installed at the endpoint of an +-shaped frame. The motors are represented as $M_i, i = 1, 2, 3, 4$ and corresponding thrust forces generated by them are $f_i, i = 1, 2, 3, 4$. The motors M_1 and M_3 spin in the clockwise direction with angular velocities ω_1 and ω_3. While the angular velocities of motors M_2 and M_4 are denoted as ω_2 and ω_4 in the counter-clockwise direction.

The states of the quadrotor UAV can be controlled by changing the angular velocities of four motors. For instance, the quadrotor hovers with certain four equal angular velocities of motors, and the quadrotor rises or descends when increasing or decreasing the angular velocities of motors simultaneously. When $f_1 \neq f_3$, the quadrotor is conducted at the working mode of pitching. And the quadrotor works at the rolling mode when $f_2 \neq f_4$.

As shown in Fig. 1, two frames are applied to describe the motion of the quadrotor. The earth-based coordinate system $\{E\}(O, x, y, z)$ is an inertial frame which is used to express the position $[x, y, z]^T$ of the quadrotor. The body-fixed coordinate system $\{B\}(O_b, x_b, y_b, z_b)$ is fixed to the center of mass of the quadrotor. The attitude angles $[\phi, \theta, \psi]^T$ between the earth-based coordinate and the body-fixed

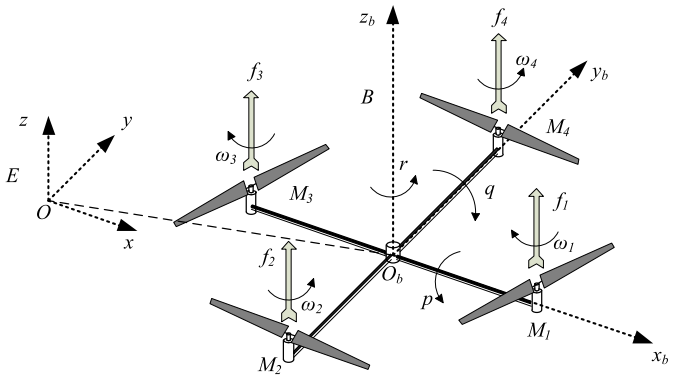

Fig. 1. Quadrotor UAVs.

coordinate describe the orientation of the body frame, where ϕ, θ and ψ represent the roll angle, pitch angle and yaw angle, respectively. The angular speeds around the axes of the body-fixed coordinate are p, q and r.

In order to simplify the model, the body frame of the quadrotor is supposed to be rigid and the structure is symmetrical in the $x_b - O_b - y_b$ plane. The drag is assumed to be linear. The process of detailed derivation of the model can be obtained from [21] and [22]. The Newton-Euler method is utilized and the quadrotor dynamics model is described by the following differential equations:

$$\begin{cases} \ddot{x} = \frac{1}{m}\left[(\cos\phi\cos\psi\sin\theta + \sin\phi\sin\psi)u_f - k_t\dot{x} + F_{dx}\right] \\ \ddot{y} = \frac{1}{m}\left[(\cos\phi\sin\theta\sin\psi - \cos\psi\sin\phi)u_f - k_t\dot{y} + F_{dy}\right] \\ \ddot{z} = \frac{1}{m}\left[(\cos\theta\cos\phi)u_f - mg - k_t\dot{z} + F_{dz}\right] \\ \dot{p} = \frac{1}{I_{xx}}[-k_r p - qr(I_{zz} - I_{yy}) + \tau_p + \Delta d_p] \\ \dot{q} = \frac{1}{I_{yy}}[-k_r q - pr(I_{xx} - I_{zz}) + \tau_q + \Delta d_q] \\ \dot{r} = \frac{1}{I_{zz}}[-k_r r - pq(I_{yy} - I_{xx}) + \tau_r + \Delta d_r] \\ \dot{\phi} = p + q\sin\phi\tan\theta + r\cos\phi\tan\theta \\ \dot{\theta} = q\cos\phi - r\sin\phi \\ \dot{\psi} = \frac{1}{\cos\theta}[q\sin\phi + r\cos\phi] \end{cases} \tag{1}$$

In equation (1), m represents the mass of the quadrotor and g is the gravity coefficient. The moments of inertia along the x_b, y_b and z_b axes are represented by I_{xx}, I_{yy} and I_{zz}, respectively. The torques around the body frame axis are described by $\left[\tau_p, \tau_q, \tau_r\right]^T$. The total lift in the z_b direction is $u_f = f_1 + f_2 + f_3 + f_4$. The translational drag coefficient and the rotational drag coefficient are k_t and k_r, respectively. The external disturbances of the system caused by the wind are represented by F_{dx}, F_{dy} and F_{dz}. And the bounded model uncertainties caused by the modeling errors are denoted as Δd_p, Δd_q and Δd_r.

The control inputs of the dynamic system (1) are expressed as $\left[u_f, \tau_p, \tau_q, \tau_r\right]^T$ while the real inputs of the quadrotor are $[f_1, f_2, f_3, f_4]^T$. And the relationship between them can be expressed as the following equation:

$$\begin{bmatrix} u_f \\ \tau_p \\ \tau_q \\ \tau_r \end{bmatrix} = \begin{bmatrix} 1 & 1 & 1 & 1 \\ 0 & -l & 0 & l \\ -l & 0 & l & 0 \\ d & -d & d & -d \end{bmatrix} \begin{bmatrix} f_1 \\ f_2 \\ f_3 \\ f_4 \end{bmatrix}. \tag{2}$$

Since the mapping (2) is bijective, we can design the quadrotor's controller with control inputs $\left[u_f, \tau_p, \tau_q, \tau_r\right]^T$. In equation (2) l is the length of the quadrotor arm, and d is the ratio between the drag and the thrust coefficients of the blade.

And the relationship between the lift forces $[f_1, f_2, f_3, f_4]^T$ and the rotational speeds of the rotors $[\omega_1, \omega_2, \omega_3, \omega_4]^T$ can be expressed as:

$$f_i = b\omega_i{}^2, \quad i = 1, 2, 3, 4 \tag{3}$$

where b is the thrust coefficient.

Due to the sensor noise, all states of the dynamic system are polluted with white noise. And the following dynamics of actuator is considered.

$$\omega_i = \frac{K}{\tau s + 1}\omega_{ci}, \quad i = 1, 2, 3, 4 \tag{4}$$

where ω_{ci} are the command of rotational speeds given by the flight controller. τ is the time constant and K is the gain of the actuator.

Without loss of generality, the failure of motor M_2 is considered in this paper. Failure of motors M_1, M_3 or M_4 can be similarly considered because of the symmetry assumption. Selecting the states of the dynamic system as:

$$\begin{aligned}\mathbf{x} &= [x_1, x_2, x_3, x_4, x_5, x_6, x_7, x_8, x_9, x_{10}, x_{11}, x_{12}]^T \\ &= [\dot{x}, \dot{y}, \dot{z}, x, y, z, p, q, r, \phi, \theta, \psi]^T,\end{aligned} \tag{5}$$

and choosing the control inputs as:

$$\begin{aligned}\mathbf{u} &= [u_1, u_2, u_3]^T \\ &= [u_f, \tau_q, \tau_r]^T.\end{aligned} \tag{6}$$

Then from (1), the following differential equations can be obtained.

$$\begin{cases}\dot{x}_1 = \frac{1}{m}[(\cos x_{10}\cos x_{12}\sin x_{11} + \sin x_{10}\sin x_{12})u_1 - k_t x_1 + F_{dx}] \\ \dot{x}_2 = \frac{1}{m}\left[(\cos x_{10}\sin x_{11}\sin x_{12} - \cos x_{12}\sin x_{10})u_1 - k_t x_2 + F_{dy}\right] \\ \dot{x}_3 = \frac{1}{m}[(\cos x_{11}\cos x_{10})u_1 - mg - k_t x_3 + F_{dz}] \\ \dot{x}_4 = x_1 \\ \dot{x}_5 = x_2 \\ \dot{x}_6 = x_3 \\ \dot{x}_7 = \frac{1}{I_{xx}}[-k_r x_7 - x_8 x_9(I_{zz} - I_{yy}) + \frac{l}{2}(u_1 - \frac{u_3}{d}) + \Delta d_p] \\ \dot{x}_8 = \frac{1}{I_{yy}}[-k_r x_8 - x_7 x_9(I_{xx} - I_{zz}) + u_2 + \Delta d_q] \\ \dot{x}_9 = \frac{1}{I_{zz}}[-k_r x_9 - x_7 x_8(I_{yy} - I_{xx}) + u_3 + \Delta d_r] \\ \dot{x}_{10} = x_7 + x_8\sin x_{10}\tan x_{11} + x_9\cos x_{10}\tan x_{11} \\ \dot{x}_{11} = x_8\cos x_{10} - x_9\sin x_{10} \\ \dot{x}_{12} = \frac{1}{\cos x_{11}}[x_8\sin x_{10} + x_9\cos x_{10}]\end{cases} \tag{7}$$

The relationship between the control inputs of dynamic system (7) and the real inputs of the quadrotor $[f_1, f_3, f_4]^T$ can now be expressed as:

$$\begin{bmatrix} u_f \\ \tau_q \\ \tau_r \end{bmatrix} = \begin{bmatrix} 1 & 1 & 1 \\ -l & l & 0 \\ d & d & -d \end{bmatrix} \begin{bmatrix} f_1 \\ f_3 \\ f_4 \end{bmatrix}, \tag{8}$$

which is still a bijective mapping.

The essential target of this paper is to design a flight controller based on NTSMC to deal with a total rotor failure. Because of the one rotor failure assumption, the control system is under-actuated and the yaw angle ψ has to be ignored according to the similar work finished by [22]. The control inputs are $\left[u_f, \tau_q, \tau_r\right]^T$ and the control objective is to make the quadrotor reach to the desired positions $[x_d, y_d, z_d]^T$ and the desired attitudes $[\phi_d, \theta_d]^T$.

3. Flight controller design

In this section, a complete fault-tolerant control system for quadrotor UAV is studied. A NTSMC based fault-tolerant flight controller with a total rotor failure is proposed and this is the first time to apply NTSMC to deal with the situation of a total rotor failure. Meanwhile, a NTSMC based fault-free flight controller is proposed which has a similar structure compared with the fault-tolerant one. Finally, a fault detection and diagnosis method is applied and two methods are then proposed to estimate the wind disturbances and model uncertainties with a total rotor failure. And the proposed NDE based estimation method is more insensitive to noise compared with the proposed SMD based method. The estimation results can be used to compensate the external disturbances and model uncertainties, in order to enhance the robustness of the proposed fault-tolerant flight controller.

3.1. Fault-tolerant controller

This subsection mainly designs a NTSMC based flight controller with a rotor failure. The double loop structure of control system is shown as Fig. 2. The outer controller takes the desired positions x_d and y_d as the reference inputs and generates the desired attitudes ϕ_d and θ_d, which are the reference inputs of the inner controller. And the inner controller produces the final control inputs u_f, τ_q and τ_r. The states of the quadrotor are supposed known by the controllers. The outer controller needs the system states x and y. And the inner controller requires the attitude related states p, q, r, ϕ, θ and ψ. Model uncertainties and external disturbances are considered.

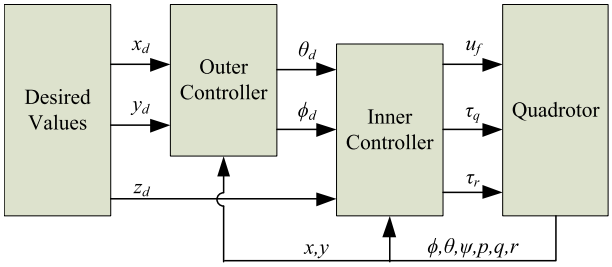

Fig. 2. Structure diagram of control system with one rotor failure.

3.1.1. Inner controller

Selecting the states of the inner control loop as $\bar{\mathbf{x}} = [\bar{x}_1, \bar{x}_2, \bar{x}_3, \bar{x}_4, \bar{x}_5, \bar{x}_6, \bar{x}_7]^T = [x_3, x_6, x_7, x_8, x_9, x_{10}, x_{11}]^T$.

From (7), the inner loop dynamic system can be obtained as:

$$\dot{\bar{\mathbf{x}}} = \mathbf{f}(\bar{\mathbf{x}}) + \mathbf{h}(\bar{\mathbf{x}})\mathbf{u} + \mathbf{g}(\bar{\mathbf{x}}), \tag{9}$$

where

$$\mathbf{f}(\bar{\mathbf{x}}) = \begin{bmatrix} \frac{1}{m}[-mg - k_t x_3] \\ x_3 \\ \frac{1}{I_{xx}}[-k_r x_7 - x_8 x_9 (I_{zz} - I_{yy})] \\ \frac{1}{I_{yy}}[-k_r x_8 - x_7 x_9 (I_{xx} - I_{zz})] \\ \frac{1}{I_{zz}}[-k_r x_9 - x_7 x_8 (I_{yy} - I_{xx})] \\ x_7 + x_8 \sin x_{10} \tan x_{11} + x_9 \cos x_{10} \tan x_{11} \\ x_8 \cos x_{10} - x_9 \sin x_{10} \end{bmatrix} \in R^{7\times 1} \tag{10}$$

$$\mathbf{h}(\bar{\mathbf{x}}) = \begin{bmatrix} \frac{1}{m}\cos x_{10} \cos x_{11} & 0 & 0 \\ 0 & 0 & 0 \\ \frac{l}{2I_{xx}} & 0 & -\frac{l}{2dI_{xx}} \\ 0 & \frac{1}{I_{yy}} & 0 \\ 0 & 0 & \frac{1}{I_{zz}} \\ 0 & 0 & 0 \\ 0 & 0 & 0 \end{bmatrix} \in R^{7\times 3} \tag{11}$$

$$\mathbf{g}(\bar{\mathbf{x}}) = \begin{bmatrix} \frac{F_{dz}}{m} \\ 0 \\ \frac{1}{I_{xx}}\Delta d_p \\ \frac{1}{I_{yy}}\Delta d_q \\ \frac{1}{I_{zz}}\Delta d_r \\ 0 \\ 0 \end{bmatrix}, \tag{12}$$

The dynamics of the states x_6, x_{10} and x_{11} can be written as:

$$\begin{bmatrix} \dot{x}_6 \\ \dot{x}_{10} \\ \dot{x}_{11} \end{bmatrix} = \begin{bmatrix} \bar{x}_1 \\ \bar{x}_3 + \bar{x}_4 \sin \bar{x}_6 \tan \bar{x}_7 + \bar{x}_5 \cos \bar{x}_6 \tan \bar{x}_7 \\ \bar{x}_4 \cos \bar{x}_6 - \bar{x}_5 \sin \bar{x}_6 \end{bmatrix} = \bar{\mathbf{f}}(\bar{\mathbf{x}}) \tag{13}$$

From (9) and (13), the following equation can be derived:

$$\begin{bmatrix} \ddot{x}_6 \\ \ddot{x}_{10} \\ \ddot{x}_{11} \end{bmatrix} = \mathbf{J}(\bar{\mathbf{x}})\mathbf{f}(\bar{\mathbf{x}}) + \mathbf{J}(\bar{\mathbf{x}})\mathbf{h}(\bar{\mathbf{x}})\mathbf{u} + \mathbf{J}(\bar{\mathbf{x}})\mathbf{g}(\bar{\mathbf{x}}), \tag{14}$$

where

$$\mathbf{J}(\bar{\mathbf{x}}) = \frac{\partial \bar{\mathbf{f}}(\bar{\mathbf{x}})}{\partial \bar{\mathbf{x}}} = \begin{bmatrix} 1 & 0 & 0 \\ 0 & 0 & 0 \\ 0 & 1 & 0 \\ 0 & \sin\bar{x}_6 \tan\bar{x}_7 & \cos\bar{x}_6 \\ 0 & \cos\bar{x}_6 \tan\bar{x}_7 & -\sin\bar{x}_6 \\ 0 & \bar{x}_4 \cos\bar{x}_6 \tan\bar{x}_7 - \bar{x}_5 \sin\bar{x}_6 \tan\bar{x}_7 & -\bar{x}_4 sin\bar{x}_6 - \bar{x}_5 \cos\bar{x}_6 \\ 0 & \frac{\bar{x}_4 \sin\bar{x}_6 + \bar{x}_5 cos\bar{x}_6}{\cos^2\bar{x}_7} & 0 \end{bmatrix}^T \tag{15}$$

Define:

$$\begin{aligned} &\mathbf{x_I} \doteq [x_6, x_{10}, x_{11}]^T \\ &\mathbf{x_{Id}} \doteq [x_{6d}, x_{10d}, x_{11d}]^T = [z_d, \phi_d, \theta_d]^T, \end{aligned} \tag{16}$$

then the sliding mode variables can be selected as:

$$\mathbf{S_I} = (\mathbf{x_I} - \mathbf{x_{Id}}) + \frac{1}{\bar{\beta}}(\dot{\mathbf{x}}_\mathbf{I} - \dot{\mathbf{x}}_\mathbf{Id})^{\bar{p}/\bar{q}}, \tag{17}$$

where $\bar{\beta} > 0$ is a constant real number and $\bar{p} > 0$ and $\bar{q} > 0$ are constant real odd numbers satisfying $1 < \bar{p}/\bar{q} < 2$.

The inner controller can be designed as the following form:

$$\begin{aligned} \mathbf{u} &= \mathbf{u^{eq}} + \mathbf{u^{dis}} \\ &= -[\mathbf{J}(\bar{\mathbf{x}})\mathbf{h}(\bar{\mathbf{x}})]^{-1}[\frac{\bar{\beta}\bar{q}}{\bar{p}}(\dot{\mathbf{x}}_\mathbf{I} - \dot{\mathbf{x}}_\mathbf{Id})^{2-\bar{p}/\bar{q}} + \mathbf{J}(\bar{\mathbf{x}})\mathbf{f}(\bar{\mathbf{x}}) + \mathbf{J}(\bar{\mathbf{x}})\hat{\mathbf{g}}(\bar{\mathbf{x}}) - \ddot{\mathbf{x}}_\mathbf{Id}] \\ &\quad - [\mathbf{J}(\bar{\mathbf{x}})\mathbf{h}(\bar{\mathbf{x}})]^{-1}[M_I \mathrm{sign}(\mathbf{S_I}) + \bar{M}_I \left\|\mathbf{J}(\bar{\mathbf{x}})\hat{\mathbf{g}}(\bar{\mathbf{x}})\right\|_\infty \mathrm{sign}(\mathbf{S_I})] \end{aligned} \tag{18}$$

where $M_I > 0$ and $\bar{M}_I > 0$ are constant real numbers, $\mathbf{u^{eq}}$ and $\mathbf{u^{dis}}$ are equivalent control part and discontinuous control part respectively. $\hat{\mathbf{g}}(\bar{\mathbf{x}})$ is the estimation result of the inner loop's external disturbances and model uncertainties $\mathbf{g}(\bar{\mathbf{x}})$.

Selecting the following Lyapunov candidate function:

$$V_I = \frac{1}{2}\mathbf{S_I}^T\mathbf{S_I} > 0 \tag{19}$$

From (17), (18) and (19), the following condition can be derived:

$$\dot{V}_I = \mathbf{S_I}^T[\frac{\bar{p}}{\bar{\beta}\bar{q}}(\dot{\mathbf{x}}_\mathbf{I} - \dot{\mathbf{x}}_\mathbf{Id})^{\bar{p}/\bar{q}-1} \circ (\mathbf{J}(\bar{\mathbf{x}})\mathbf{g}(\bar{\mathbf{x}}) - \mathbf{J}(\bar{\mathbf{x}})\hat{\mathbf{g}}(\bar{\mathbf{x}}) - M_I \mathrm{sign}(\mathbf{S_I}) - \bar{M}_I \left\|\mathbf{J}(\bar{\mathbf{x}})\hat{\mathbf{g}}(\bar{\mathbf{x}})\right\|_\infty \mathrm{sign}(\mathbf{S_I}))] \tag{20}$$

According to the Lyapunov stability theory, $\dot{V}_I$ should be negative definite. Because of every element of vector $\bar{p}/\bar{\beta}\bar{q} \cdot (\dot{\mathbf{x}}_\mathbf{I} - \dot{\mathbf{x}}_\mathbf{Id})^{\bar{p}/\bar{q}-1}$ is not less than 0, the stability condition of the inner control loop can be obtained as:

$$M_I > 0 \tag{21}$$

and

$$\bar{M}_I > \frac{\left\|\mathbf{J}(\bar{\mathbf{x}})\mathbf{g}(\bar{\mathbf{x}}) - \mathbf{J}(\bar{\mathbf{x}})\hat{\mathbf{g}}(\bar{\mathbf{x}})\right\|_\infty}{\left\|\mathbf{J}(\bar{\mathbf{x}})\hat{\mathbf{g}}(\bar{\mathbf{x}})\right\|_\infty} \tag{22}$$

From (20), (21) and (22), the following relationship can be derived:

$$\dot{V}_I < 0, \tag{23}$$

which completes the stability analysis. Then, after entering the sliding mode surface, from (17) the finite settling time can be derived as:

$$T_I \leq \|\mathbf{x_I} - \mathbf{x_{Id}}\|^{1-\bar{q}/\bar{p}}/(\bar{\beta}^{\bar{q}/\bar{p}}(1 - \bar{q}/\bar{p})). \tag{24}$$

3.1.2. Outer controller

Selecting the states of the outer control loop as $\tilde{\mathbf{x}} = \left[\tilde{x}_1, \tilde{x}_2, \tilde{x}_3, \tilde{x}_4\right]^T = [x_1, x_2, x_4, x_5]^T$. From (7), the outer loop dynamics can be described as:

$$\begin{bmatrix} \dot{\tilde{x}}_1 \\ \dot{\tilde{x}}_2 \\ \dot{\tilde{x}}_3 \\ \dot{\tilde{x}}_4 \end{bmatrix} = \begin{bmatrix} \frac{1}{m}\left[(\cos x_{10}\cos x_{12}\sin x_{11} + \sin x_{10}\sin x_{12})u_1 - k_t\tilde{x}_1 + F_{dx}\right] \\ \frac{1}{m}\left[(\cos x_{10}\sin x_{11}\sin x_{12} - \cos x_{12}\sin x_{10})u_1 - k_t\tilde{x}_2 + F_{dy}\right] \\ \tilde{x}_1 \\ \tilde{x}_2 \end{bmatrix} \tag{25}$$

Assume that the inner loop runs faster than the outer loop, and define:

$$\begin{aligned} &\mathbf{x_O} \doteq [x_4, x_5]^T \\ &\mathbf{x_{Od}} \doteq [x_{4d}, x_{5d}]^T = [x_d, y_d]^T. \end{aligned} \tag{26}$$

The outer loop dynamic (25) can be further simplified as:

$$\begin{aligned} \ddot{\mathbf{x}}_\mathbf{O} = &-\tfrac{k_t}{m}\dot{\mathbf{x}}_\mathbf{O} + \tfrac{1}{m}\begin{bmatrix} F_{dx} \\ F_{dy} \end{bmatrix} \\ &+\tfrac{u_1}{m}\begin{bmatrix} \sin x_{12} & \cos x_{12} \\ -\cos x_{12} & \sin x_{12} \end{bmatrix}\begin{bmatrix} x_{10d} + \Delta\phi \\ x_{11d} + \Delta\theta \end{bmatrix}, \end{aligned} \tag{27}$$

and $[\phi_d, \theta_d]^T = [x_{10d}, x_{11d}]^T$, generated by the outer controller, are the reference inputs of the inner controller. In equation (27) $\Delta\phi$ and $\Delta\theta$ represent the tracking errors of ϕ_d and θ_d, respectively. They can be expressed as the following equations.

$$\Delta\phi = \phi - \phi_d \tag{28}$$

$$\Delta\theta = \theta - \theta_d \tag{29}$$

We further assume that the boundaries of tracking errors are d_ϕ and d_θ, which means $|\Delta\phi| \le d_\phi$ and $|\Delta\theta| \le d_\theta$. Note that the stability proof of the inner controller makes it reasonable to make such an assumption.

The sliding mode variables can be selected as:

$$\mathbf{S_O} = (\mathbf{x_O} - \mathbf{x_{Od}}) + \frac{1}{\tilde{\beta}}(\dot{\mathbf{x}}_\mathbf{O} - \dot{\mathbf{x}}_\mathbf{Od})^{\tilde{p}/\tilde{q}}, \tag{30}$$

where $\tilde{\beta} > 0$ is a constant real number and $\tilde{p} > 0$ and $\tilde{q} > 0$ are constant real odd numbers satisfying $1 < \tilde{p}/\tilde{q} < 2$.

The outer controller can be designed as the following form:

$$\begin{aligned} \begin{bmatrix} x_{10d} \\ x_{11d} \end{bmatrix} &= \tilde{\mathbf{u}} \\ &= \tilde{\mathbf{u}}^{\mathbf{eq}} + \tilde{\mathbf{u}}^{\mathbf{dis}} \\ &= -\frac{m}{u_1}\begin{bmatrix} \sin x_{12} & -\cos x_{12} \\ \cos x_{12} & \sin x_{12} \end{bmatrix}[-\frac{k_t}{m}\dot{\mathbf{x}}_\mathbf{O} \\ &\quad + \frac{1}{m}\begin{bmatrix} \hat{F}_{dx} \\ \hat{F}_{dy} \end{bmatrix} - \ddot{\mathbf{x}}_\mathbf{Od} + \frac{\tilde{\beta}\tilde{q}}{\tilde{p}}(\dot{\mathbf{x}}_\mathbf{O} - \dot{\mathbf{x}}_\mathbf{Od})^{2-\tilde{p}/\tilde{q}}] \\ &\quad - \frac{m}{u_1}\begin{bmatrix} \sin x_{12} & -\cos x_{12} \\ \cos x_{12} & \sin x_{12} \end{bmatrix} M_O \cdot \mathrm{sign}(\mathbf{S_O}) \\ &\quad - \frac{m}{u_1}\bar{M}_O\begin{bmatrix} \sin x_{12} & -\cos x_{12} \\ \cos x_{12} & \sin x_{12} \end{bmatrix}\cdot\begin{bmatrix} \left|\hat{F}_{dx}\right| & 0 \\ 0 & \left|\hat{F}_{dy}\right| \end{bmatrix}\mathrm{sign}(\mathbf{S_O}) \end{aligned} \tag{31}$$

where $M_O > 0$ and $\bar{M}_O > 0$ are constant real numbers. $\hat{F}_{dx}$ and $\hat{F}_{dy}$ represent the estimation results of the wind disturbances F_{dx} and F_{dy}, respectively. $\tilde{\mathbf{u}}^{\mathbf{eq}}$ and $\tilde{\mathbf{u}}^{\mathbf{dis}}$ are equivalent control part and discontinuous control part respectively.

Selecting the following Lyapunov candidate function:

$$V_O = \frac{1}{2}\mathbf{S_O}^T\mathbf{S_O} > 0 \tag{32}$$

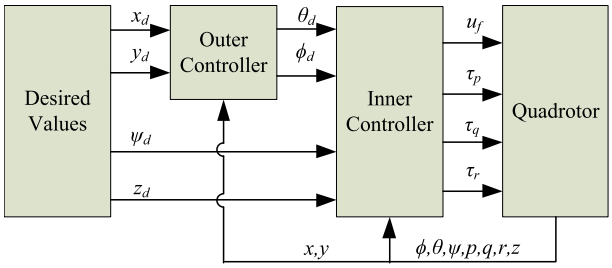

Fig. 3. Fault-free structure diagram of control system.

From (30), (31) and (32), the following condition can be derived:

$$\begin{aligned}\dot{V}_O = {} & \mathbf{S_O}^T [\tfrac{\tilde{p}}{\tilde{\beta}\tilde{q}} (\dot{\mathbf{x}}_\mathbf{O} - \dot{\mathbf{x}}_\mathbf{Od})^{\tilde{p}/\tilde{q}-1} \\ & \circ [\tfrac{1}{m} \begin{bmatrix} F_{dx} - \hat{F}_{dx} \\ F_{dy} - \hat{F}_{dy} \end{bmatrix} - M_O \operatorname{sign}(\mathbf{S_O}) \\ & - \bar{M}_O \begin{bmatrix} \left|\hat{F}_{dx}\right| & 0 \\ 0 & \left|\hat{F}_{dy}\right| \end{bmatrix} \operatorname{sign}(\mathbf{S_O}) \\ & + \tfrac{u_1}{m} \begin{bmatrix} \sin x_{12} & \cos x_{12} \\ -\cos x_{12} & \sin x_{12} \end{bmatrix} \begin{bmatrix} \Delta\phi \\ \Delta\theta \end{bmatrix}]]\end{aligned} \tag{33}$$

According to the Lyapunov stability theory, $\dot{V}_O$ should be negative definite. Because of every element of vector $\tilde{p}/\tilde{\beta}\tilde{q} \cdot (\dot{\mathbf{x}}_\mathbf{O} - \dot{\mathbf{x}}_\mathbf{Od})^{\tilde{p}/\tilde{q}-1}$ is not less than 0, the stability condition of the inner control loop can be obtained as:

$$\begin{cases} M_O > \left|\frac{F_{dx} - \hat{F}_{dx}}{m}\right| + \left|\frac{u_1}{m} d_\phi\right| + \left|\frac{u_1}{m} d_\theta\right| \\ M_O > \left|\frac{F_{dy} - \hat{F}_{dy}}{m}\right| + \left|\frac{u_1}{m} d_\phi\right| + \left|\frac{u_1}{m} d_\theta\right| \end{cases} \tag{34}$$

and

$$\bar{M}_O > 0. \tag{35}$$

From (33), (34) and (35), the following relationship can be derived:

$$\dot{V}_O < 0, \tag{36}$$

which completes the stability analysis. Then, after entering the sliding mode surface, from (30) the finite settling time can be derived as:

$$T_O \leq \|\mathbf{x_O} - \mathbf{x_{Od}}\|^{1-\tilde{q}/\tilde{p}} / (\tilde{\beta}^{\tilde{q}/\tilde{p}} (1 - \tilde{q}/\tilde{p})). \tag{37}$$

3.2. Fault-free controller

This subsection designs a fault-free flight controller based on NTSMC. The control structure is selected as similar as the fault-tolerant one. To guarantee the succinctness of the paper, we only list the fault-free controllers and the corresponding stability conditions here since the designing process is similar with the fault-tolerant case in the previous subsection.

Fig. 3, which is similar to Fig. 2, shows the structure diagram of the control system with the healthy rotors. The only difference between Fig. 2 and Fig. 3 is that the yaw angle is controllable in the fault-free case, and it is controlled by the inner controller.

Different from the fault-tolerant inner controller, the fault-free controller includes two parts: the attitude controller and the height controller. The control objective of the attitude controller is to make quadrotor follow the desired attitude $[\phi_d, \theta_d, \psi_d]^T$. And the height controller can make the quadrotor track the desired height z_d.

Selecting the states of the attitude inner control loop as:

$\bar{\mathbf{x}}_\mathbf{H} = [x_7, x_8, x_9, x_{10}, x_{11}, x_{12}]^T = [\bar{x}_{H1}, \bar{x}_{H2}, \bar{x}_{H3}, \bar{x}_{H4}, \bar{x}_{H5}, \bar{x}_{H6}]^T$, and choosing the control input as:

$$\mathbf{u_H} = [\tau_p, \tau_q, \tau_r]^T. \tag{38}$$

From (7), the inner loop dynamic system can be obtained as:

$$\dot{\bar{\mathbf{x}}}_\mathbf{H} = \mathbf{f_H}(\bar{\mathbf{x}}_\mathbf{H}) + \mathbf{h_H}(\bar{\mathbf{x}}_\mathbf{H})\mathbf{u_H} + \mathbf{g_H}(\bar{\mathbf{x}}_\mathbf{H}), \tag{39}$$

where

$$\mathbf{f_H}(\bar{\mathbf{x}}_\mathbf{H}) = \begin{bmatrix} \frac{1}{I_{xx}}[-k_r x_7 - x_8 x_9 (I_{zz} - I_{yy})] \\ \frac{1}{I_{yy}}[-k_r x_8 - x_7 x_9 (I_{xx} - I_{zz})] \\ \frac{1}{I_{zz}}[-k_r x_9 - x_7 x_8 (I_{yy} - I_{xx})] \\ x_7 + x_8 \sin x_{10} \tan x_{11} + x_9 \cos x_{10} \tan x_{11} \\ x_8 \cos x_{10} - x_9 \sin x_{10} \\ \frac{1}{\cos x_{10}}[x_8 \sin x_{10} + x_9 \cos x_{10}] \end{bmatrix} \in R^{6\times 1} \tag{40}$$

$$\mathbf{h_H}(\bar{\mathbf{x}}_\mathbf{H}) = \begin{bmatrix} \frac{1}{I_{xx}} & 0 & 0 \\ 0 & \frac{1}{I_{yy}} & 0 \\ 0 & 0 & \frac{1}{I_{zz}} \\ 0 & 0 & 0 \\ 0 & 0 & 0 \\ 0 & 0 & 0 \end{bmatrix} \in R^{6\times 3} \tag{41}$$

$$\mathbf{g_H}(\bar{\mathbf{x}}_\mathbf{H}) = \begin{bmatrix} \frac{1}{I_{xx}} \Delta d_p \\ \frac{1}{I_{yy}} \Delta d_q \\ \frac{1}{I_{zz}} \Delta d_r \\ 0 \\ 0 \\ 0 \end{bmatrix} \in R^{6\times 1} \tag{42}$$

The dynamics of the states x_{10}, x_{11} and x_{12} can be written as:

$$\begin{bmatrix} \dot{x}_{10} \\ \dot{x}_{11} \\ \dot{x}_{12} \end{bmatrix} = \begin{bmatrix} \bar{x}_{H1} + \bar{x}_{H2} \sin \bar{x}_{H4} \tan \bar{x}_{H5} + \bar{x}_{H3} \cos \bar{x}_{H4} \tan \bar{x}_{H5} \\ \bar{x}_{H2} \cos \bar{x}_{H4} - \bar{x}_{H3} \sin \bar{x}_{H4} \\ \frac{1}{\cos \bar{x}_{H5}}[\bar{x}_{H2} \sin \bar{x}_{H4} + \bar{x}_{H3} \cos \bar{x}_{H4}] \end{bmatrix} = \bar{\mathbf{f}}_\mathbf{H}(\bar{\mathbf{x}}_\mathbf{H}) \tag{43}$$

From (39) and (43), the following equation can be derived:

$$\begin{bmatrix} \ddot{x}_{10} \\ \ddot{x}_{11} \\ \ddot{x}_{12} \end{bmatrix} = \mathbf{J_H}(\bar{\mathbf{x}}_\mathbf{H}) \mathbf{f_H}(\bar{\mathbf{x}}_\mathbf{H}) + \mathbf{J_H}(\bar{\mathbf{x}}_\mathbf{H}) \mathbf{h_H}(\bar{\mathbf{x}}_\mathbf{H}) \mathbf{u_H} + \mathbf{J_H}(\bar{\mathbf{x}}_\mathbf{H}) \mathbf{g_H}(\bar{\mathbf{x}}_\mathbf{H}), \tag{44}$$

where

$$\begin{aligned} \mathbf{J}(\bar{\mathbf{x}}) &= \frac{\partial \bar{\mathbf{f}}(\bar{\mathbf{x}})}{\partial \bar{\mathbf{x}}} \\ &= \begin{bmatrix} 1 & 0 & 0 \\ \sin \bar{x}_4 \tan \bar{x}_5 & \cos \bar{x}_4 & \frac{\sin \bar{x}_4}{\cos \bar{x}_5} \\ \cos \bar{x}_4 \tan \bar{x}_5 & -\sin \bar{x}_4 & \frac{\cos \bar{x}_4}{\cos \bar{x}_5} \\ \bar{x}_2 \cos \bar{x}_4 \tan \bar{x}_5 - \bar{x}_3 \sin \bar{x}_4 \tan \bar{x}_5 & -\bar{x}_2 \sin \bar{x}_4 - \bar{x}_3 \cos \bar{x}_4 & \frac{\bar{x}_2 \cos \bar{x}_4 - \bar{x}_3 \sin \bar{x}_4}{\cos \bar{x}_5} \\ \frac{\bar{x}_2 \sin \bar{x}_4 + \bar{x}_3 \cos \bar{x}_4}{\cos^2 \bar{x}_5} & 0 & \frac{\sin \bar{x}_5 [\bar{x}_2 \sin \bar{x}_4 + \bar{x}_3 \cos \bar{x}_4]}{\cos^2 \bar{x}_5} \\ 0 & 0 & 0 \end{bmatrix}^T \end{aligned} \tag{45}$$

Define:

$$\begin{aligned} &\mathbf{x_{IH}} \doteq [x_{10}, x_{11}, x_{12}]^T \\ &\mathbf{x_{IHd}} \doteq [x_{10d}, x_{11d}, x_{12d}]^T = [\phi_d, \theta_d, \psi_d]^T, \end{aligned} \tag{46}$$

then the sliding mode variables can be selected as:

$$\mathbf{S_{IH}} = (\mathbf{x_{IH}} - \mathbf{x_{IHd}}) + \frac{1}{\bar{\beta}_H} (\dot{\mathbf{x}}_\mathbf{IH} - \dot{\mathbf{x}}_\mathbf{IHd})^{\bar{p}_H/\bar{q}_H}, \tag{47}$$

where $\bar{\beta}_H > 0$ is a constant real number and $\bar{p}_H > 0$ and $\bar{q}_H > 0$ are constant real odd numbers satisfying $1 < \bar{p}_H/\bar{q}_H < 2$.

The inner controller can be designed as the following form:

$$\begin{aligned}\mathbf{u_H} &= \mathbf{u_H}^{\mathbf{eq}} + \mathbf{u_H}^{\mathbf{dis}} \\ &= -[\mathbf{J_H}(\bar{\mathbf{x}}_\mathbf{H})\mathbf{h_H}(\bar{\mathbf{x}}_\mathbf{H})]^{-1}[\frac{\bar{\beta}_H \bar{q}_H}{\bar{p}_H}(\dot{\mathbf{x}}_\mathbf{IH} - \dot{\mathbf{x}}_\mathbf{IHd})^{2-\bar{p}_H/\bar{q}_H} + \mathbf{J_H}(\bar{\mathbf{x}}_\mathbf{H})\mathbf{f_H}(\bar{\mathbf{x}}_\mathbf{H}) - \ddot{\mathbf{x}}_\mathbf{IHd}] \\ &\quad - [\mathbf{J_H}(\bar{\mathbf{x}}_\mathbf{H})\mathbf{h_H}(\bar{\mathbf{x}}_\mathbf{H})]^{-1} M_{IH}\,\mathrm{sign}(\mathbf{S_{IH}})\end{aligned} \tag{48}$$

where $M_{IH} > 0$ is a constant real number, $\mathbf{u_H}^{\mathbf{eq}}$ and $\mathbf{u_H}^{\mathbf{dis}}$ are equivalent control part and discontinuous control part respectively.

Selecting the following Lyapunov candidate function:

$$V_{IH} = \frac{1}{2}\mathbf{S_{IH}}^T\mathbf{S_{IH}} > 0 \tag{49}$$

According to the Lyapunov theory, the following stability condition can be obtained:

$$M_{IH} > \|\mathbf{J_H}(\bar{\mathbf{x}}_\mathbf{H})\mathbf{g_H}(\bar{\mathbf{x}}_\mathbf{H})\|_\infty \tag{50}$$

From (47), (48), (49) and (50), the following relationship can be finally derived:

$$\dot{V}_{IH} < 0. \tag{51}$$

After entering the sliding mode surface, from (47) the finite settling time can be derived as:

$$T_{IH} \le \|\mathbf{x_{IH}} - \mathbf{x_{IHd}}\|^{1-\bar{q}_H/\bar{p}_H}/(\bar{\beta}_H^{\bar{q}_H/\bar{p}_H}(1-\bar{q}_H/\bar{p}_H)). \tag{52}$$

Then, we need to design the height controller.

The following dynamic process of the height can be obtained from (1).

$$\ddot{z} = \frac{1}{m}\left[(\cos\theta\cos\phi)u_f - mg - k_t\dot{z} + F_{dz}\right] \tag{53}$$

The sliding mode surface is selected as:

$$S_z = (z - z_d) + \frac{1}{\beta_z}(\dot{z} - \dot{z}_d)^{p_z/q_z} \tag{54}$$

where z_d is the desired height, $\beta_z > 0$ is a constant real number and p_z and q_z are constant real odd numbers satisfying $1 < p_z/q_z < 2$.

Then the height controller $u_z = u_f$ is designed as:

$$\begin{aligned}u_z &= {u_z}^{eq} + {u_z}^{dis} \\ &= -\tfrac{m}{\cos\theta\cos\phi}[-\tfrac{k_t}{m}\dot{z} - g - \ddot{z}_d + \tfrac{1}{m}\hat{F}_{dz} + \tfrac{\beta_z q_z}{p_z}(\dot{z} - \dot{z}_d)^{2-p_z/q_z}] \\ &\quad -\tfrac{m}{\cos\theta\cos\phi}M_Z\,sign(S_z)\end{aligned} \tag{55}$$

where $\hat{F}_{dz}$ is the estimation result of the wind disturbance F_{dz} and $M_z > 0$ is a constant real number.

The Lyapunov candidate function is selected as:

$$V_z = \frac{1}{2}{S_z}^2 \tag{56}$$

According to the Lyapunov theory, the following stability condition can be obtained:

$$M_z > \left|\frac{1}{m}(F_{dz} - \hat{F}_{dz})\right| \tag{57}$$

From (54), (55), (56) and (57), the following relationship can be finally derived:

$$\dot{V}_z < 0. \tag{58}$$

Then, after entering the sliding mode surface, from (54) the finite settling time can be derived as:

$$T_{zH} \le |z - z_d|^{1-q_z/p_z}/(\beta_z{}^{q_z/p_z}(1 - q_z/p_z)). \tag{59}$$

The fault-free outer controller is identical to the fault-tolerant outer controller derived in the subsection 3.1. Hence it will not be repeated here.

3.3. Fault detection and diagnosis method

Inspired by [27], the following fault detection and diagnosis method is applied in this paper.

$$\begin{bmatrix} \hat{l}_1 \\ \hat{l}_2 \\ \hat{l}_1 \\ \hat{l}_4 \end{bmatrix} = \begin{bmatrix} 1 \\ 1 \\ 1 \\ 1 \end{bmatrix} - A^{-1} \begin{bmatrix} \hat{u}_f \\ \hat{\tau}_p \\ \hat{\tau}_q \\ \hat{\tau}_r \end{bmatrix} \tag{60}$$

where

$$A = \begin{bmatrix} b{\omega_1}^2 & 1 & 1 & 1 \\ 0 & -lb{\omega_2}^2 & 0 & l \\ -l & 0 & lb{\omega_3}^2 & 0 \\ d & -d & d & -db{\omega_4}^2 \end{bmatrix} \tag{61}$$

$\hat{u}_f$, $\hat{\tau}_p$, $\hat{\tau}_q$ and $\hat{\tau}_r$ are the estimated u_f, τ_p, τ_q and τ_r, and the detailed method can be found in [27]. When $\hat{l}_i = 0, i = 1, 2, 3, 4$, there is no rotor failure. And $\hat{l}_i = 1$ when the ith rotor is totally failed.

3.4. Wind disturbances and model uncertainties estimator

3.4.1. Wind disturbances estimator

In this paper, inspired by [40], the following NDE based wind disturbance estimator is proposed for the UAV system. We assumed that the positions, velocities and attitude angles information of the UAVs are accessable, but they are polluted by gaussian white noise. For ease of description, we only depict the wind disturbance estimator of F_{dx} here. The similar nonlinear disturbance estimator can be derived to estimate F_{dy} and F_{dz} in the same way, which we don't list here. The NDE based wind disturbance estimator can be described as:

$$\hat{F}_{dx} = \hat{a}_x - \frac{1}{m}\left[(\cos\hat{\phi}\cos\hat{\psi}\sin\hat{\theta} + \sin\hat{\phi}\sin\hat{\psi})\hat{u}_f - k_t\hat{v}_x\right] \tag{62}$$

where $\hat{a}_x$ and $\hat{v}_x$ are the estimation results of the acceleration and speed of the UAV in the x direction, respectively. Similarly, $\hat{\phi}$, $\hat{\psi}$ and $\hat{\theta}$ are the estimation results of the attitude angles. And $\hat{u}_f$ is the filtered u_f. All estimated states can be obtained from the following estimator [40]:

$$\begin{aligned} \dot{\hat{x}}_1 &= \hat{x}_2 \\ \dot{\hat{x}}_2 &= \hat{x}_3 \\ \dot{\hat{x}}_3 &= (s - \hat{x}_1)\cdot\bar{\omega}_2^2\bar{\omega}_1 - (\bar{\omega}_2^2 + 2\zeta\bar{\omega}_2\bar{\omega}_1)\hat{x}_2 - (2\zeta\bar{\omega}_2 + \bar{\omega}_1)\hat{x}_3 \\ \hat{s} &= \hat{x}_1 \\ \dot{\hat{s}} &= \hat{x}_2 \\ \ddot{\hat{s}} &= \hat{x}_3 \end{aligned} \tag{63}$$

where $\hat{x}_1$, $\hat{x}_2$ and $\hat{x}_3$ are auxiliary variables. $\bar{\omega}_1$, $\bar{\omega}_2$ and ζ are the designed parameters. s is the measured state of the UAV. $\hat{s}$, $\dot{\hat{s}}$ and $\ddot{\hat{s}}$ are the estimation results of s, $\dot{s}$ and $\ddot{s}$, respectively. For instance, if let $s := x$, then $\hat{v}_x = \dot{\hat{s}} = \hat{x}_2$ and $\hat{a}_x = \ddot{\hat{s}} = \hat{x}_3$. If let $s := \phi$, then $\hat{\phi} = \hat{x}_1$.

For comparison, the following sliding mode differentiator (SMD) [28] is also applied to estimate the wind disturbance, which might be sensitive to the noise of the system.

$$\begin{aligned} \delta\dot{x} &= \dot{x} - \dot{\hat{x}} \\ \ddot{\hat{x}} &= \frac{1}{m}\left[(\cos\phi\cos\psi\sin\theta + \sin\phi\sin\psi)u_f - k_t\dot{x}\right] \\ \dot{\eta}_0 &= \eta_1 - \mu_0|\eta_0 - \delta\dot{x}|^{\frac{1}{2}}sign(\eta_0 - \delta\dot{x}) \\ \dot{\eta}_1 &= -\mu_1 sign(\eta_1 - \dot{\eta}_0) \\ \hat{F}_{dx} &= \eta_1 \end{aligned} \tag{64}$$

where $\hat{x}$, η_0, η_1 are auxiliary variables. μ_0 and μ_1 are designed variables. Note that SMD (64) only gets the estimation result of F_{dx}. The similar SMD can also be derived to estimate F_{dy} and F_{dz}, which we also don't list here.

3.4.2. Model uncertainties estimator

Similar with (62), the following NDE based model uncertainties estimator is proposed.

$$\hat{\mathbf{g}}(\bar{\mathbf{x}}) = \hat{\dot{\bar{\mathbf{x}}}} - \mathbf{f}(\hat{\bar{\mathbf{x}}}) - \mathbf{h}(\hat{\bar{\mathbf{x}}})\hat{\mathbf{u}} \tag{65}$$

where $\hat{\dot{\bar{\mathbf{x}}}}$ is the estimation result of $\dot{\bar{\mathbf{x}}}$, $\hat{\bar{\mathbf{x}}}$ and $\hat{\mathbf{u}}$ are the estimation results of $\bar{\mathbf{x}}$ and $\mathbf{u}$, respectively. All estimated states can be obtained from the following estimator [40]:

$$\begin{aligned}
\dot{\hat{\mathbf{x}}}_{\mathbf{1}} &= \hat{\mathbf{x}}_{\mathbf{2}} \\
\dot{\hat{\mathbf{x}}}_{\mathbf{2}} &= \hat{\mathbf{x}}_{\mathbf{3}} \\
\dot{\hat{\mathbf{x}}}_{\mathbf{3}} &= (\bar{\mathbf{x}} - \hat{\mathbf{x}}_{\mathbf{1}})\cdot\bar{\omega}_2^2\bar{\omega}_1 - (\bar{\omega}_2^2 + 2\zeta\bar{\omega}_2\bar{\omega}_1)\hat{\mathbf{x}}_{\mathbf{2}} - (2\zeta\bar{\omega}_2 + \bar{\omega}_1)\hat{\mathbf{x}}_{\mathbf{3}} \\
\hat{\bar{\mathbf{x}}} &= \hat{\mathbf{x}}_{\mathbf{1}} \\
\hat{\dot{\bar{\mathbf{x}}}} &= \hat{\mathbf{x}}_{\mathbf{2}}
\end{aligned} \tag{66}$$

where $\hat{\mathbf{x}}_1, \hat{\mathbf{x}}_{\mathbf{2}}, \hat{\mathbf{x}}_{\mathbf{3}} \in \mathbf{R}^7$ are auxiliary variables. $\bar{\omega}_1$, $\bar{\omega}_2$ and ζ are the designed parameters.

For comparison, the following SMD is also applied to estimate the model uncertainties, which might be sensitive to the noise of the system.

$$\begin{aligned}
\delta\bar{\mathbf{x}} &= \bar{\mathbf{x}} - \hat{\bar{\mathbf{x}}} \\
\hat{\dot{\bar{\mathbf{x}}}} &= \mathbf{f}(\bar{\mathbf{x}}) + \mathbf{h}(\bar{\mathbf{x}})\mathbf{u} \\
\dot{\eta}_{\mathbf{0}} &= \eta_{\mathbf{1}} - \mu_0|\eta_{\mathbf{0}} - \delta\bar{x}|^{\frac{1}{2}}\circ\mathrm{sign}(\eta_{\mathbf{0}} - \delta\bar{\mathbf{x}}) \\
\dot{\eta}_{\mathbf{1}} &= -\mu_1\mathrm{sign}(\eta_{\mathbf{1}} - \dot{\eta}_{\mathbf{0}}) \\
\hat{\mathbf{g}}(\bar{\mathbf{x}}) &= \eta_{\mathbf{1}}
\end{aligned} \tag{67}$$

where $\hat{\bar{\mathbf{x}}}, \eta_{\mathbf{0}}, \eta_{\mathbf{1}} \in R^7$ are auxiliary variables. μ_0 and μ_1 are designed variables.

3.5. Chattering reduction

Because that the sliding mode control is applied in this paper to design the flight controller, the chattering phenomenon is an inevitable problem. To solve the chattering problem to some extent, the following smooth functions are applied to replace the sign functions in the proposed controllers.

$$\begin{aligned}
\mathrm{sgmf}(\mathbf{S_I}) &= 2\left(\frac{1}{1+e^{-\alpha\mathbf{S_I}}} - \frac{1}{2}\right) \\
\mathrm{sgmf}(\mathbf{S_O}) &= 2\left(\frac{1}{1+e^{-\alpha\mathbf{S_O}}} - \frac{1}{2}\right)
\end{aligned} \tag{68}$$

where $\alpha > 0$ is a constant real number. The replacement appears when $|\mathbf{S_I}| < \varepsilon$ or $|\mathbf{S_O}| < \varepsilon$, and ε is a small constant positive real number which should be selected inversely proportional to α.

4. Simulation results

In this section, numerical simulation results are performed to demonstrate the performance of the proposed NTSMC based fault-tolerant flight controller. Three methods are simulated and compared: 1) the pure NTSMC based controller; 2) the NTSMC based controller with the SMD based estimator (NTSMC-SMD); 3) the NTSMC based controller with the nonlinear disturbance estimator based estimator (NTSMC-NDE).

Two simulation cases are considered in this section. One case is that the quadrotor faces a sudden total failure of one rotor when flying normally, in order to verify the effectiveness of the FDD method and the fault-tolerant controller. Another case is that the quadrotor encounters a wind disturbance with a rotor total failure, in order to show the strong robustness of the proposed fault-tolerant controller and the disturbance estimator.

To be closer to the real model of the quadrotor, all states of the UAV system are polluted with white noise. And the dynamics of actuator (4) is considered.

The main parameters used in the simulation part are presented as follows. The mass of the quadrotor is $m = 0.5kg$, the arm length is $L = 0.255m$. The inertia of the quadrotor are $I_{xx} = I_{yy} = 5.9 \times 10^{-3} kg \cdot m^2$ and $I_{zz} = 1.16 \times 10^{-2} kg \cdot m^2$. The translational drag coefficient and the rotational drag coefficient are $k_r = k_t = 6 \times 10^{-3}$. The thrust and torque coefficients are $b = 3.13 \times 10^{-5}, d = 4.8 \times 10^{-3}$.

4.1. Sudden failure case

The model parameters have 70% errors at maximum and the rotor M_2 is completely failed after 8s. And more disturbances are added to the inner loop after the failure happened. The simulation results of NTSMC, NTSMC-SMD and NTSMC-NDE are shown in Fig. 4, Fig. 5 and Fig. 6. The rotor M_2 completely failed after 8s and Fig. 4 show that the proposed NTSMC based fault-tolerant flight controller can stabilize the quadrotor after fault happened. Fig. 4(c) shows that FDD woks normally since l_2 becomes 1 from 0 after 8s, which means

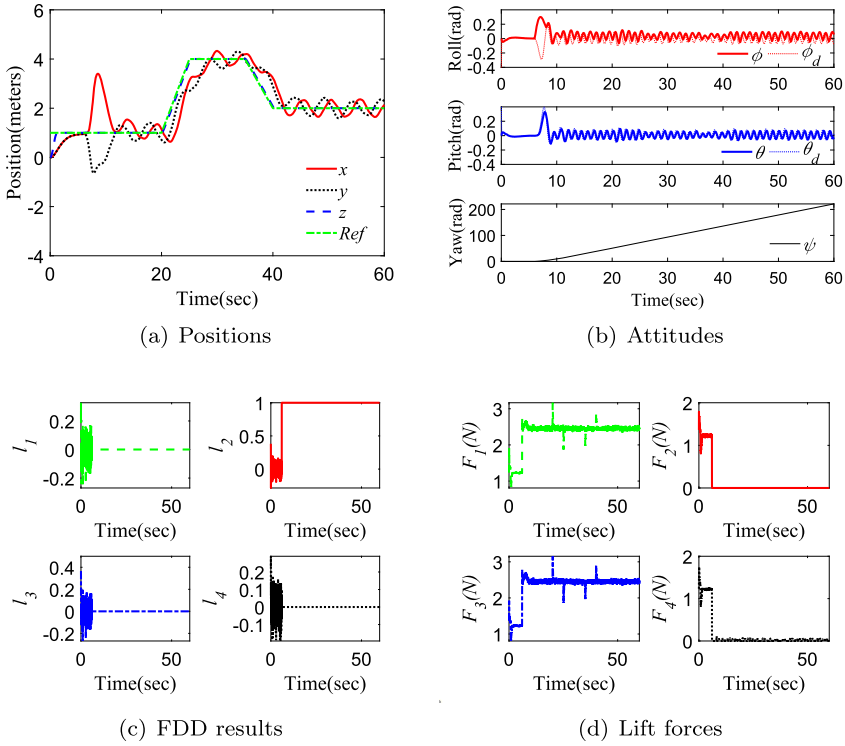

(a) Positions (b) Attitudes

(c) FDD results (d) Lift forces

Fig. 4. Sudden failure simulation results of NTSMC.

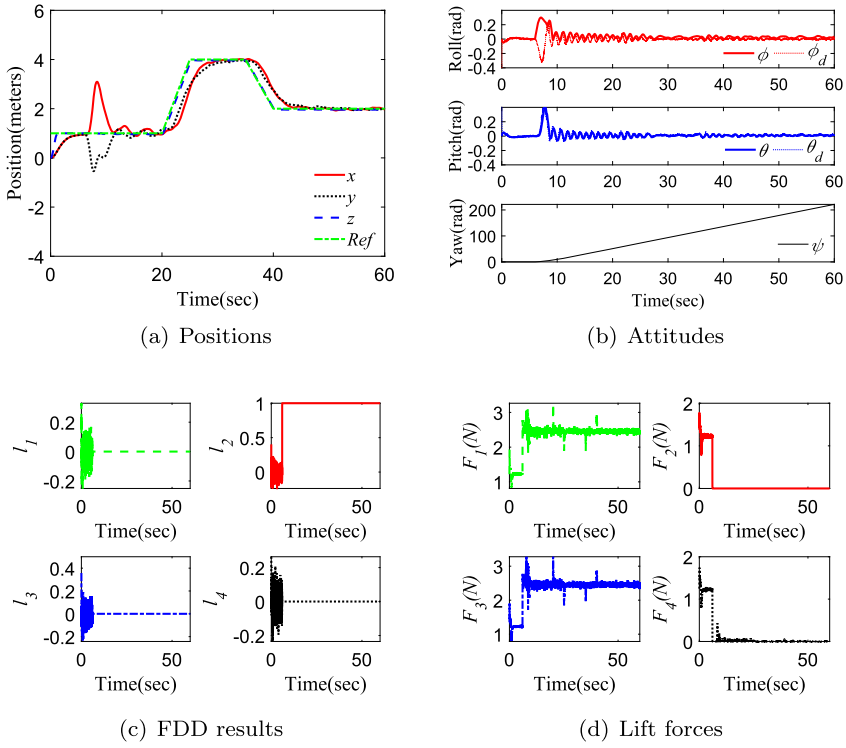

(a) Positions (b) Attitudes

(c) FDD results (d) Lift forces

Fig. 5. Sudden failure simulation results of NTSMC-SMD.

that the fault is detected and the flight controller is reconfigured from the fault-free controller to the fault-tolerant controller. From Fig. 4(a) Fig. 5(a) Fig. 6(a) and Fig. 7, we can obtain that the proposed NTSMC-SMD and NTSMC-NDE also work well when one total rotor failure happens. What is more, NTSMC-SMD and NTSMC-NDE perform better compared with pure NTSMC, because that NTSMC-SMD and NTSMC-NDE compensate the model uncertainties of the system. However, since SMD is sensitive to the noise of the system, NTSMC-SMD have more severe chattering phenomenon compared with NTSMC-NDE, as shown in Fig. 5(b) and Fig. 6(b). From Fig. 4(b) and Fig. 6(b), we can conclude that NTSMC-NDE needs less attitude changing compared with pure NTSMC.

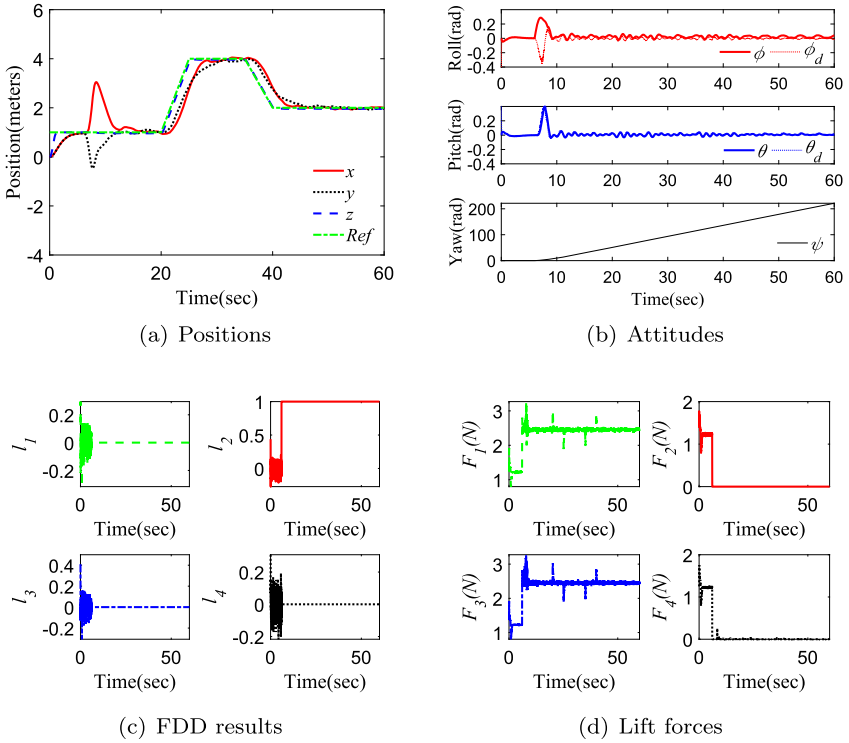

Fig. 6. Sudden failure simulation results of NTSMC-NDE.

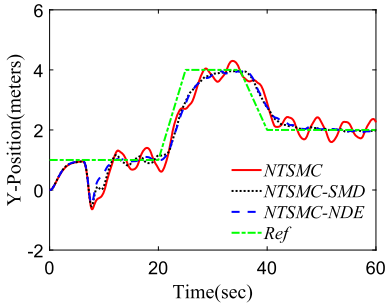

Fig. 7. Y position.

4.2. Wind disturbances case

The model parameters have 70% errors at maximum. And more disturbances are added to the inner loop. The rotor M_2 is completely failed from the beginning and the lateral wind disturbances are added between 40s to 50s as the following form: $F_{dx} = 0.25 + 0.1\sin t + 0.1\cos t$, $F_{dy} = -0.25 - 0.1\sin t - 0.1\cos t$.

Fig. 8(a) shows that the pure NTSMC based flight controller can not handle this external disturbance well. While Fig. 9(a) and Fig. 10(a) show that the proposed NTSMC controller has s stronger robustness if the wind disturbances are estimated and compensated into the controller. NTSMC-SMD and NTSMC-NDE can handle the wind disturbances well. However, SMD is more sensitive to the system's noise compared with the proposed nonlinear disturbance estimator, which can be obtained from Fig. 9(c) and Fig. 10(c). The estimation RMSE of SMD and NDE are shown in Fig. 12. As a result, NTSMC-NDE achieves less chattering performance on the attitudes control results compared with NTSMC-SMD, which can be obtained from Fig. 9(b) and Fig. 10(b). Numerical simulation results show the great performance of the proposed flight control method. (See Fig. 11.)

The total rotor failure problem is challenging to a certain extent. Because that we can only use three rotors to control the quadrotor. The yaw angle is uncontrollable in such a case. We can obtained from Fig. 4(b), Fig. 5(b), Fig. 6(b), Fig. 8(b), Fig. 9(b) and Fig. 10(b) that the yaw angles are diverging, which means that the quadrotor is spinning. We need to control the position of the quadrotor under the condition that the attitude is not totally controllable.

For the same reason, the requirement of FDD is tough. If the FDD works slowly, the quadrotor will crash because that the fault-tolerant controller can't replace the fault-free controller timely. From our failure simulations, the states of the quadrotor will diverge if the FDD can't give the right information within about 10ms.

A complete fault-tolerant control system is studied in this paper, which copes with not only fault detection and isolation but also fault-tolerant control. And the simulation results shows strong robustness of the proposed method, which has some practical value in engineering application, since some engineering problems have been considered in this paper. To be closer to the real model of the quadrotor, all states of the UAV system are polluted with white noise. The dynamics of actuators are considered in the simulation part and

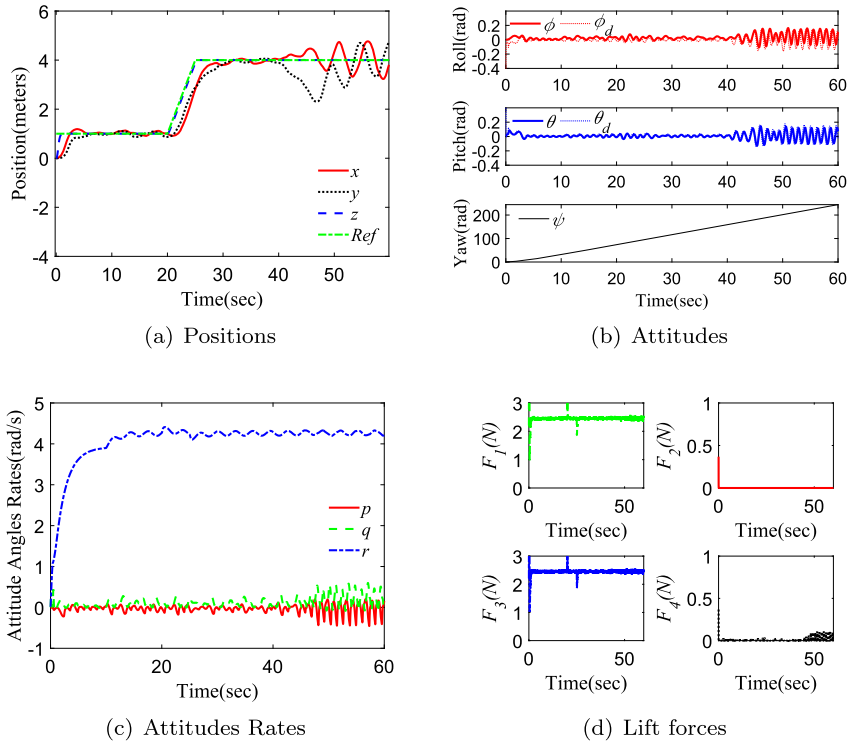

(a) Positions (b) Attitudes

(c) Attitudes Rates (d) Lift forces

Fig. 8. Wind disturbance simulation results of NTSMC.

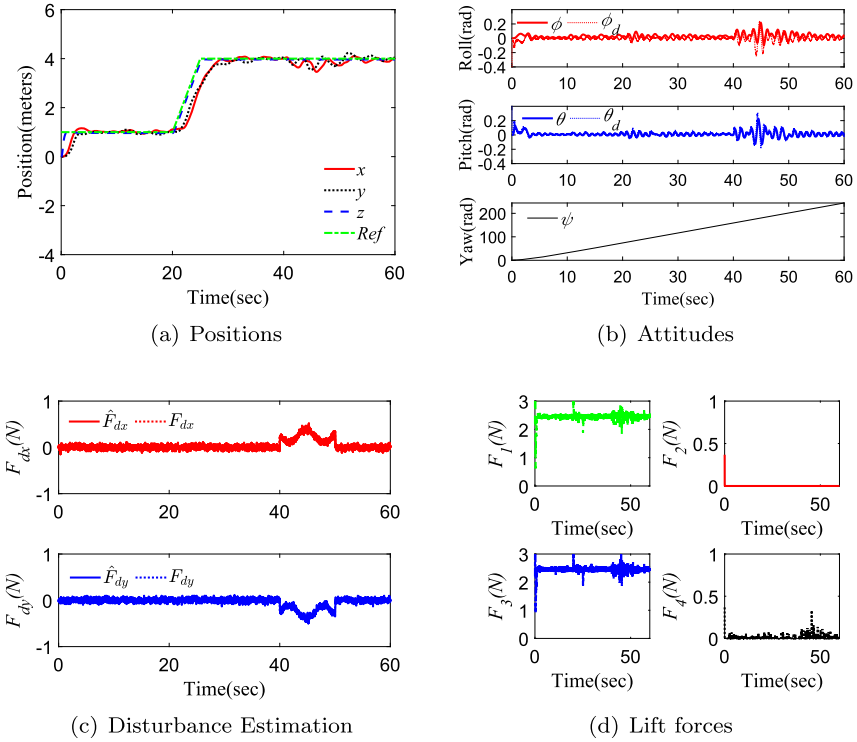

(a) Positions (b) Attitudes

(c) Disturbance Estimation (d) Lift forces

Fig. 9. Wind disturbance simulation results of NTSMC-SMD.

the model parameters are assumed having 70% errors at maximum. The wind disturbances are also considered in this paper. Considering the above uncertainties and disturbances, the proposed NTSMC-NDE method shows strong robustness and better control performance compared with pure NTSMC method. The NTSMC-NDE method shows less sensitivity to the system's noise and achieves less chattering performance on the attitudes control results compared with NTSMC-SMD method.

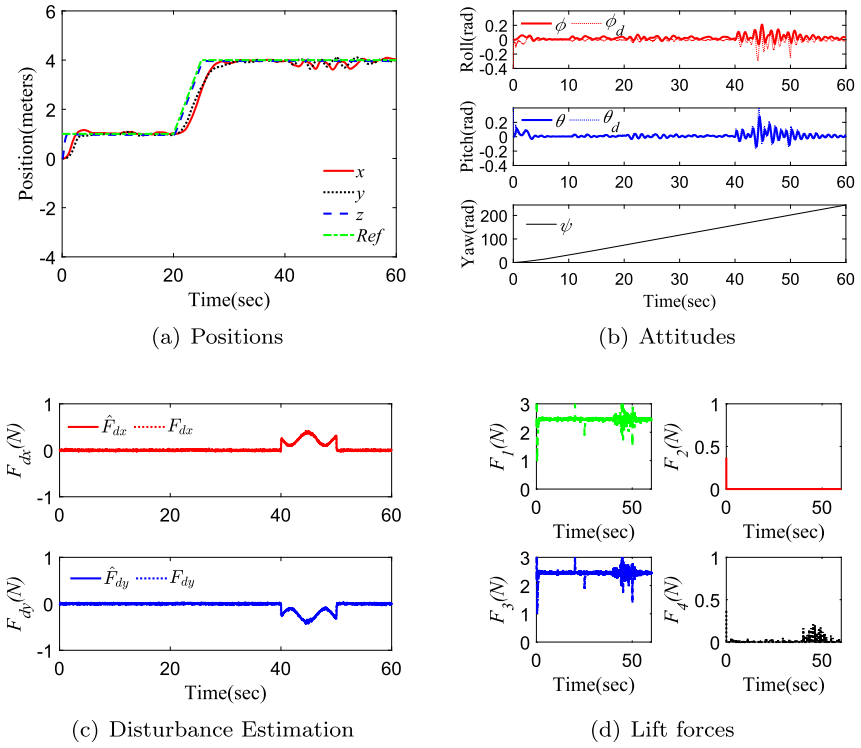

Fig. 10. Wind disturbance simulation results of NTSMC-NDE.

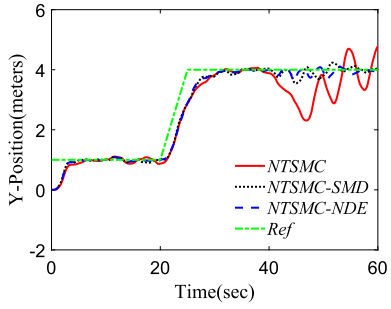

Fig. 11. Y position.

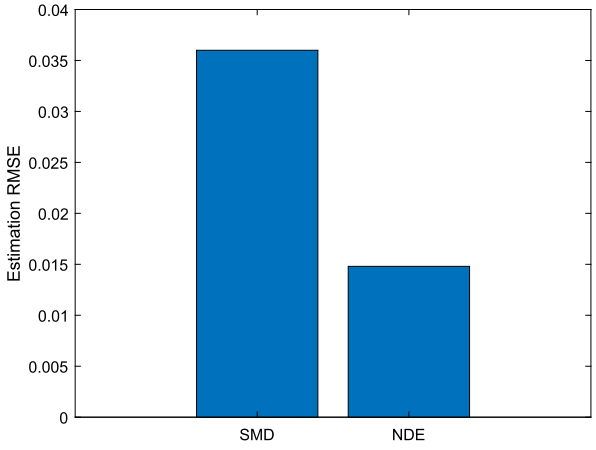

Fig. 12. RMSE of estimation.

5. Conclusions

A fault-tolerant flight controller is proposed in this paper for a quadrotor with a total rotor failure based on nonsingular terminal sliding mode control. The proposed method is a finite-time position and attitude tracking approach with strong robustness. A complete fault-tolerant control system is studied in this paper, which copes with not only fault detection and isolation but also fault-tolerant control. Besides, the model uncertainties and wind disturbances are considered. Two different methods are utilized to estimate the external disturbances and model uncertainties in real time. It is the first time that we use NDE to estimate the wind disturbance and model uncertainties acting on the quadrotor. We compare the NDE-based estimator with SMD and show that the NDE-based estimator is more insensitive to noise. In future work, the practical hardware experiments will be considered.

Declaration of competing interest

The authors declare that they have no known competing financial interests or personal relationships that could have appeared to influence the work reported in this paper.

Acknowledgements

This work is supported by the Foundation Committee of Basic and Applied Basic Research of Guangdong Province (Fund No. 2019A1515011252) and the Hong Kong University Grants Committee (UGC) Fund under Grant 1-BE24.

References

[1] H. Bolandi, M. Rezaei, R. Mohsenipour, H. Nemati, S.M. Smailzadeh, Attitude control of a quadrotor with optimized pid controller, Intell. Control Autom. 4 (03) (2013) 335.
[2] S. Gonzalez-Vazquez, J. Moreno-Valenzuela, A new nonlinear pi/pid controller for quadrotor posture regulation, in: 2010 IEEE Electronics, Robotics and Automotive Mechanics Conference, IEEE, 2010, pp. 642–647.
[3] P. Ghiglino, J.L. Forshaw, V.J. Lappas, Online pid self-tuning using an evolutionary swarm algorithm with experimental quadrotor flight results, in: AIAA Guidance, Navigation, and Control (GNC) Conference, 2013, p. 5098.
[4] J. Ma, R. Ji, Fuzzy pid for quadrotor space fixed-point position control, in: 2016 Sixth International Conference on Instrumentation & Measurement, Computer, Communication and Control, IMCCC, IEEE, 2016, pp. 721–726.
[5] G.V. Raffo, M.G. Ortega, F.R. Rubio, An integral predictive/nonlinear h∞ control structure for a quadrotor helicopter, Automatica 46 (1) (2010) 29–39.
[6] H. Jafarnejadsani, D. Sun, H. Lee, N. Hovakimyan, Optimized l 1 adaptive controller for trajectory tracking of an indoor quadrotor, J. Guid. Control Dyn. 40 (6) (2017) 1415–1427.
[7] J. Hwangbo, I. Sa, R. Siegwart, M. Hutter, Control of a quadrotor with reinforcement learning, IEEE Robot. Autom. Lett. 2 (4) (2017) 2096–2103.
[8] C. Wang, J. Wang, X. Zhang, X. Zhang, Autonomous navigation of UAV in large-scale unknown complex environment with deep reinforcement learning, in: 2017 IEEE Global Conference on Signal and Information Processing, GlobalSIP, IEEE, 2017, pp. 858–862.
[9] W. Lou, X. Guo, Adaptive trajectory tracking control using reinforcement learning for quadrotor, Int. J. Adv. Robot. Syst. 13 (1) (2016) 38.
[10] H. Wang, X. Ye, Y. Tian, G. Zheng, N. Christov, Model-free–based terminal smc of quadrotor attitude and position, IEEE Trans. Aerosp. Electron. Syst. 52 (5) (2016) 2519–2528.
[11] J.-J. Xiong, G.-B. Zhang, Global fast dynamic terminal sliding mode control for a quadrotor UAV, ISA Trans. 66 (2017) 233–240.
[12] Y. Zhang, A. Chamseddine, C.A. Rabbath, B.W. Gordon, C.-Y. Su, S. Rakheja, C. Fulford, J. Apkarian, P. Gosselin, Development of advanced fdd and ftc techniques with application to an unmanned quadrotor helicopter testbed, J. Franklin Inst. 350 (9) (2013) 2396–2422.
[13] E. Kiyak, A. Kahvecioglu, F. Caliskan, Aircraft sensor and actuator fault detection, isolation, and accommodation, J. Aerosp. Eng. 24 (1) (2010) 46–58.
[14] M. Mohammadi, A.M. Shahri, Adaptive nonlinear stabilization control for a quadrotor UAV: theory, simulation and experimentation, J. Intell. Robot. Syst. 72 (1) (2013) 105–122.
[15] X. Zhang, Y. Zhang, C.-Y. Su, Y. Feng, Fault-tolerant control for quadrotor UAV via backstepping approach, in: 48th AIAA Aerospace Sciences Meeting Including the New Horizons Forum and Aerospace Exposition, 2010, p. 947.
[16] P. Lu, E.-J. van Kampen, Q.P. Chu, Nonlinear quadrotor control with online model identification, in: Advances in Aerospace Guidance, Navigation and Control, Springer, 2015, pp. 81–98.
[17] I. Sadeghzadeh, A. Mehta, Y. Zhang, Fault/damage tolerant control of a quadrotor helicopter UAV using model reference adaptive control and gain-scheduled PID, in: AIAA Guidance, Navigation, and Control Conference, 2011, p. 6716.
[18] A. Chamseddine, Y. Zhang, C.-A. Rabbath, J. Apkarian, C. Fulford, Model reference adaptive fault tolerant control of a quadrotor UAV, in: Infotech@ Aerospace 2011, 2011, p. 1606.
[19] A. Tayebi, S. McGilvray, Attitude stabilization of a vtol quadrotor aircraft, IEEE Trans. Control Syst. Technol. 14 (3) (2006) 562–571.
[20] B. Crowther, A. Lanzon, M. Maya-Gonzalez, D. Langkamp, Kinematic analysis and control design for a nonplanar multirotor vehicle, J. Guid. Control Dyn. 34 (4) (2011) 1157–1171.
[21] A. Freddi, A. Lanzon, S. Longhi, A feedback linearization approach to fault tolerance in quadrotor vehicles, IFAC Proc. Vol. 44 (1) (2011) 5413–5418.
[22] A. Lanzon, A. Freddi, S. Longhi, Flight control of a quadrotor vehicle subsequent to a rotor failure, J. Guid. Control Dyn. 37 (2) (2014) 580–591.
[23] M.W. Mueller, R. D'Andrea, Stability and control of a quadrocopter despite the complete loss of one, two, or three propellers, in: 2014 IEEE International Conference on Robotics and Automation, ICRA, IEEE, 2014, pp. 45–52.
[24] V. Lippiello, F. Ruggiero, D. Serra, Emergency landing for a quadrotor in case of a propeller failure: a pid based approach, in: IEEE International Symposium on Safety, 2014.
[25] V. Lippiello, F. Ruggiero, D. Serra, Emergency landing for a quadrotor in case of a propeller failure: a backstepping approach, in: 2014 IEEE/RSJ International Conference on Intelligent Robots and Systems, 2014, pp. 4782–4788.
[26] S. Sun, L.M.C. Sijbers, X. Wang, C.D. Visser, High-speed flight of quadrotor despite loss of single rotor, IEEE Robot. Autom. Lett. 99 (2018) 3201–3207.
[27] P. Lu, E.J.V. Kampen, Active fault-tolerant control for quadrotors subjected to a complete rotor failure, in: IEEE/RSJ International Conference on Intelligent Robots and Systems, 2015, pp. 4073–4698.
[28] Y. Shtessel, C. Edwards, L. Fridman, A. Levant, Sliding Mode Control and Observation, Springer, 2014.
[29] M. Zak, Terminal attractors for addressable memory in neural networks, Phys. Lett. A 133 (1–2) (1988) 18–22.
[30] M. Zhihong, X.H. Yu, Terminal sliding mode control of mimo linear systems, in: Proceedings of 35th IEEE Conference on Decision and Control, vol. 4, IEEE, 1996, pp. 4619–4624.
[31] F. Yong, X. Yu, Z. Man, Non-singular terminal sliding mode control of rigid manipulators ☆, Automatica 38 (12) (2002) 2159–2167.
[32] Y. Feng, X. Yu, F. Han, On nonsingular terminal sliding-mode control of nonlinear systems ☆, Automatica 49 (2013) 1715–1722.
[33] Z. Zhao, C. Li, J. Yang, S. Li, Output feedback continuous terminal sliding mode guidance law for missile-target interception with autopilot dynamics, Aerosp. Sci. Technol. 86 (2019) 256–267.
[34] Z. Hou, L. Liu, Y. Wang, Time-to-go estimation for terminal sliding mode based impact angle constrained guidance, Aerosp. Sci. Technol. 71 (2017) 685–694.

[35] Z. Hou, L. Liu, Y. Wang, J. Huang, H. Fan, Terminal impact angle constraint guidance with dual sliding surfaces and model-free target acceleration estimator, IEEE Trans. Control Syst. Technol. 25 (1) (2016) 85–100.
[36] Z. Hou, Y. Yang, L. Liu, Y. Wang, Terminal sliding mode control based impact time and angle constrained guidance, Aerosp. Sci. Technol. 93 (2019) 1–10, https://doi.org/10.1016/j.ast.2019.04.050.
[37] X. Yin, B. Wang, L. Liu, Y. Wang, Disturbance observer-based gain adaptation high-order sliding mode control of hypersonic vehicles, Aerosp. Sci. Technol. 89 (2019) 19–30.
[38] M. Vahdanipour, M. Khodabandeh, Adaptive fractional order sliding mode control for a quadrotor with a varying load, Aerosp. Sci. Technol. 86 (2019) 737–747.
[39] X. Wang, S. Sun, E.-J. van Kampen, Q. Chu, Quadrotor fault tolerant incremental sliding mode control driven by sliding mode disturbance observers, Aerosp. Sci. Technol. 87 (2019) 417–430.
[40] P. Lu, T. Sandy, J. Buchli, Nonlinear disturbance attenuation control of hydraulic robotics, in: IEEE International Conference on Robotics and Biomimetics, 2018, pp. 1451–1458.